HHS Public Access

Author manuscript

Nat Struct Mol Biol. Author manuscript; available in PMC 2020 March 05.

Published in final edited form as:

Nat Struct Mol Biol. 2019 September ; 26(9): 816–822. doi:10.1038/s41594-019-0276-0.

Integrating spatiotemporal features of a ligand-regulated, multi-state allosteric protein

John H. Lewis, **Zhe Lu**[1]

Department of Physiology, Perelman School of Medicine, University of Pennsylvania, Philadelphia, PA 19104

Summary

Dynamic protein molecules are defined by their spatiotemporal characteristics and should thus be represented by models incorporating both characteristics. Structural biology enables determination of atomic structures of individual conformational states of a given protein. Obtaining the complementary temporal information of a given time resolution, which can be directly linked to the corresponding atomic structures, requires identifying at each time point the specific conformational state adopted by the protein. Here, we examine individual RCK domains in the regulatory module of the MthK channel by monitoring in real time the orientation of an α-helix that is conformational-state-specific. The acquired dynamic information that specifies an RCK domain's multi-state conformational changes, combined with already available corresponding atomic structures, enables us to establish an experiment-based spatiotemporal representation of an RCK domain, and to deduce a quantitative mechanistic model of the channel.

Introduction

Most proteins undergo functionally important conformational changes. These changes are defined in terms of their spatial and temporal characteristics, the knowledge of which is required to achieve a full mechanistic understanding of a protein. Structural biologists have determined angstrom-resolution three-dimensional structures of individual conformational states for a large number of proteins[1]. Recent advances in cryo-electron microscopy are accelerating the process of structure determination[2]. To complement this progress in structural biology and to transition from a static to a dynamic approach, we need relatively general approaches to directly determine the lifetimes of individual conformational states of a given protein and the connectivity among the states over the observed time. These temporal measurements can be used to relate individual structural states, only if the measurement at each time point also contains the spatial information that can unambiguously identify the specific conformational state adopted by the protein.

1 Corresponding author.

Author Contributions

J.H.L and Z.L. designed the study; J.H.L performed experiments, developed analytical tools, and analyzed the data, with the input from Z.L.; J.H.L. and Z.L. interpreted the results and wrote the manuscript.

Competing Interests

There are no competing interests.

We currently lack general, effective techniques to directly examine protein conformational kinetics at single-molecule level, in a manner that allows unambiguously linking a given kinetic state at each time point to a specific structural conformation among multiple possible conformations that the protein may adopt. This deficiency is partly because protein-conformational changes are not only rapid but also often occur on an angstrom scale, too small to be reliably and quantitatively resolved in real time. Protein conformational changes have been probed using a fluorescence resonance energy transfer (FRET) -based method, which allows the deduction of distance between a fluorescence donor and a acceptor, generally on a nanometer scale[3]. However, such deduction requires knowing the actual fluorescence transfer efficiency, which is often difficult to assess because it depends on the local environment and, in most cases, on the relative orientation of the fluorophore pair. When a protein exists in multiple states, resolution and unambiguous identification of conformational states are even more challenging.

By quantitatively resolving fluorescence-polarization changes of a bifunctional fluorophore attached to a protein[4, 5], we are able to monitor the protein's multi-state angstrom-scale conformational changes on a millisecond scale. Our test protein is the regulatory module of the MthK channel, formed by two stacked ring-like structures, each of which comprises four RCK (regulator of conductance to K^+) domains. RCK can adopt three conformational states, $\mathcal{S}_1$, $\mathcal{S}_2$ and $\mathcal{S}_3$ (Fig. 1a), which have been determined crystallographicallly[6, 7]. Ca^{2+} binds to RCK domains and regulates the conformational changes in the regulatory module, activating the channel by markedly shortening the lifetime of the closed state and modestly lengthening the lifetime of its open state[8, 9]. Single-channel current-recording approaches allow us to follow the open or closed states of the channel gate but not the conformational state of its regulatory module[10, 11]. Our fluorescence-based study has revealed that, in the isolated regulatory module, individual RCK domains independently transition among $\mathcal{S}_1$, $\mathcal{S}_2$ and $\mathcal{S}_3$, and Ca^{2+} binding to RCK promotes $\mathcal{S}_2$ over $\mathcal{S}_1$ and $\mathcal{S}_3$[4, 5] (all notations are listed in Supplementary Note 1). A minimal model of six states, three with and three without Ca^{2+} bound, is required to account for the behavior of RCK. On the basis of the characteristics of RCK, we deduced an energetic model that quantitatively predicts the dependence of the channel's open probability (p_o) on the Ca^{2+} concentration[5].

Here we set out to determine the temporal characteristics of RCK's conformational states and integrate them with the existing structural information, thereby creating a spatiotemporal representation for RCK, from which we deduce a mechanistic model for the whole channel.

Results

Dynamic behaviors of an RCK domain

To examine conformational dynamics of the RCK domain, we monitored helix αB that is located close to the channel gate and adopts a unique spatial orientation in each of the three states determined crystallographicallly[6, 7]. We monitored the polarized fluorescence emitted by a single bifunctional rhodamine molecule, attached to the α-helix in one of the eight RCK domains within the isolated regulatory module[4, 5]. Fig. 1b shows consecutive images of the emission from a single fluorophore attached to a regulatory module, recorded under a (nominal) Ca^{2+}-free condition with a camera over a constant 20 ms interval per frame,

which was split according to 0°, 45°, 90° and 135° polarizations. The integrated values of the four intensities (Fig 1c) were used to calculate inclination (θ) and rotation (φ) angles of the fluorophore's dipole in a particular conformational state, as well as the overall angle change (Ω) between two conformational states (Fig. 1d). The lines in Fig. 1c,d, color-coded for states, were generated by setting the amplitude of a given event uniformly to the average of the observed values within that event, a procedure that enhanced the effective signal-to-noise ratio and thus angle resolution on the basis of events. Starting and end points of a particular state (i.e., an event) were determined from concurrent changes among four intensities (Fig. 1c), with a method based on the *changepoint* algorithm, and the specific state, S_1, S_2 or S_3, was identified using a method based on a *k-mean-clustering* algorithm (Methods)[4].

From Ω traces, containing both θ and φ information, we obtained temporal information regarding RCK's conformational states. On the basis of this information, we generated a movie of RCK's conformational changes by matching the states that we identified at each given time point to their corresponding atomic structures in the form of electron density maps[6, 7], without any kinetic or structural modeling. Supplementary Video 1 features a single RCK domain within the regulatory module, which is presented in two views, with the module's central axis parallel (top) or perpendicular to (bottom) the plane of the page; a set of consecutive frames from the movie is shown in Fig. 1e. The temporal template of the movie was obtained from the Ω trace, part of which is shown in Fig. 1d, and the conformational states are shown in the form of electron density maps[6, 7], colored as in Fig 1a.

Ca^{2+}-dependent conformational kinetics of RCK

An experiment-based kinetic model that satisfactorily accounts for the observed conformational changes of RCK is the temporal basis for building a spatiotemporal model, defined by the number and connectivity of states, rate constants for all state transitions, and K_D values of Ca^{2+} for individual states. We describe below how we determine those rate constants from the observed state dwell times, based on the probabilities of individual state-to-state transitions. For clarity, we use the terms of dwell times and lifetime to refer to individual measurements and their mean value, respectively.

Fig. 2a shows the distributions of individual dwell times of RCK observed in S_1, S_2 or S_3 for four Ca^{2+} concentrations, measured from data traces similar to those shown in Fig. 1. If the dwell times follow a single exponential distribution, the maximum-likelihood estimate of the lifetime ($^{obs}\tau_i$) of state i can be calculated using the arithmetic mean of individual dwell times. We used an equation for data recorded with a camera at a constant frame rate (Eq. 13 in Supplementary Note 2), which also addresses the problem arising from missing short events[12]. We directly calculated the $^{obs}\tau_i$ value for each state in a given Ca^{2+} concentration and, for illustration, we also calculated single-exponential curves (Fig. 2a) from $^{obs}\tau_i$ using Eq. 12 (Supplementary Note 2). All resulting $^{obs}\tau_i$ values are plotted against the Ca^{2+} concentration in Fig. 2b.

In the absence of Ca^{2+}, the lifetime of a given state is defined by the rate constants of transitions from that state to its two neighboring states (Fig. 2c, left). We can determine the

rate constants for those transitions from their relative probabilities and lifetimes. For example, S_2 might transition to either S_1 or S_3 with probability $p_{2,1}$ or $p_{2,3}$ For these parallel transitions, the total effective rate of exiting S_2 (k_2) would be the sum of rate constants $k_{2,1}$ and $k_{2,3}$. Generally, the rate (k_i) of state S_i transitioning to either of its neighboring states S_j or S_k together is expressed as:

$$k_i = k_{i,j} + k_{i,k} = \frac{1}{\tau_i} \tag{1}$$

where $k_{i,j}$ and $k_{i,k}$ manifest themselves in accordance with:

$$k_{i,j} = \frac{1}{\tau_i} p_{i,j} \text{ and } k_{i,k} = \frac{1}{\tau_i}\left(1 - p_{i,j}\right) \tag{2}$$

Rate constants $k_{i,j}$ and $k_{i,k}$ could therefore be determined from the observed lifetime τ_i in a Ca^{2+}-free condition (Fig. 2b), once the respective state-to-state transition probabilities ($p_{i,j}$) were determined. We calculated $p_{i,j}$ (Fig. 3a) from the ratio of the number of S_i-to-S_j transitions ($n_{i,j}$) and the total number of S_i events ($N_i = n_{i,j} + n_{i,k}$):

$$p_{i,j} = \frac{n_{i,j}}{N_i};\ p_{i,k} = \frac{n_{i,k}}{N_i} \tag{3}$$

From the above relations, we obtained the following equation for direct calculation of $k_{i,j}$ from experimentally determined τ_i, $n_{i,j}$ and N_i:

$$k_{i,j} = \frac{1}{\tau_i}\frac{n_{i,j}}{N_i} \text{ and } k_{i,k} = \frac{1}{\tau_i}\frac{n_{i,k}}{N_i} \tag{4}$$

On the basis of these relations, we calculated rate constants for all Ca^{2+}concentrations (Fig. 3b).

We could obtain the rate constants $k_{i,j}$ and ${}^{ca}k_{i,j}$ for the Ca^{2+}-free and Ca^{2+}-bound forms (S_i and $S_i.Ca^{2+}$) either from apparent lifetimes ${}^{obs}\tau_i$ ($1/{}^{obs}k_i$) for zero and saturating Ca^{2+} conditions or from analyzing the entire plots in Fig. 3b. Because the Ca^{2+}-binding process is generally near the diffusion limit, S_i and $S_i.Ca^{2+}$ should be in rapid equilibrium such that the Ca^{2+}-binding kinetics would be irrelevant within the time scale of the present measurements. Thus, when S_i transitions to S_j, observed S_i (${}^{obs}S_i$) might have been in either a Ca^{2+}-free (S_i) or Ca^{2+}-bound ($S_i.Ca^{2+}$) state. In the presence of Ca^{2+}, the apparent rate constant (${}^{obs}k_{i,j}$) for state S_i transitioning to S_j can be expressed as:

$${}^{obs}k_{i,j} = \frac{k_{i,j} + {}^{ca}k_{i,j}\dfrac{\left[Ca^{2+}\right]^{n_1}}{K_{Di}}}{1 + \dfrac{\left[Ca^{2+}\right]^{n_1}}{K_{Di}}} \tag{5}$$

where the K_D of a given state i is defined by:

$$K_{Di} = \frac{[S_i]\left[Ca^{2+}\right]^{n_1}}{\left[S_i \cdot \left(Ca^{2+}\right)_{n_1}\right]} \quad (6)$$

Fitting Eq. 5 to all plots in Fig. 3b yielded the 12 rate constants in the model shown in Fig 2c, with or without Ca^{2+} bound ($k_{i,j}$ and ${}^{ca}k_{i,j}$; Supplementary Table 1). To maintain a common set of K_D values between kinetic and thermodynamic analyses, we constrained them with those obtained from analyzing the Ca^{2+} dependence of state probabilities[5] (Supplementary Table 2).

A spatiotemporal model of the isolated regulatory module

With the temporal information and existing structural data of RCK's conformational states in hand, we can now create an integrated spatiotemporal model for the eight RCK domains that independently undergo conformational changes in an isolated regulatory module. To produce a set of temporal templates, we simulated the time courses of concurrent, independent transitions for eight RCK domains in different Ca^{2+} concentrations. For a given Ca^{2+} concentration, the initial state in the simulation was randomly drawn from a trinomial distribution of the three states, S_1, S_2 and S_3, which was built according to probabilities p_1, p_2 and p_3 (calculated as previously described[5]). From that initial state (say S_2), a simulated dwell time (t_{sim}) was obtained by randomly drawing from an exponential dwell-time distribution defined by ${}^{obs}k_2$ (calculated with Eq. 17 in Supplementary Note 3, with parameters specified in Supplementary Table 1). As the simulation progressed in constant discrete 20-ms increments, the RCK domain remained in S_2 until the accumulated time of this event was greater than or equal to t_{sim}. At this point, the RCK domain in S_2 transitioned to either S_1 or S_3, based on the outcome of a random draw from a binomial distribution defined by the relative probabilities of S_2 exiting to S_1 versus S_3 ($p_{2,1}$ or $1 - p_{2,1}$; Eq. 3). The t_{sim} of this second event and its termination point were determined as described above. These steps were repeated until the entire simulation was completed. At a given Ca^{2+} concentration, Ca^{2+} occupancy in an RCK domain was determined by a random draw from a binomial distribution defined by the probabilities (p_{Bj} and $1 - p_{Bj}$) of the Ca^{2+} site being occupied and not occupied:

$$p_{Bj} = \frac{1}{\left(1 + \frac{\left[Ca^{2+}\right]^{n_1}}{K_{Dj}}\right)} \quad (7)$$

Fig. 4a shows a 5-sec segment of a 30-min simulated time course of state-to-state transitions for each of the eight RCK domains (A through H; Fig. 4b) in the regulatory domain in 0 mM Ca^{2+}. Repeating this for all experimental Ca^{2+} conditions, we calculated $\tau_{i,j}$ for each of the six transitions of RCK from the 100,000 simulated data points (Fig. 4c). For all Ca^{2+} concentrations examined, the calculated lifetimes from the simulations (open symbols) reasonably matched the corresponding experimental data points (closed symbols). The state

probabilities calculated from the simulations were also comparable to experimentally determined ones (Fig. 4d). This general good agreement between experimental data and outcomes of simulations validates the simulated temporal templates.

Together, the kinetic information obtained here and crystal structures already available together allowed us to create an experiment-based, virtual spatiotemporal "replica" of the regulatory module, in the form of a movie (Supplementary Video 2); Fig 4e shows 16 consecutive frames for 0 mM Ca^{2+}. Following the simulated time courses for three Ca^{2+} conditions, individual RCK domains transition independently among S_1, S_2 and S_3 (represented by their respective crystal structures, in two views); Ca^{2+} occupancy was determined as described above. This movie is as an effective way to exhibit the integrated model, which is fully defined by:

- **i.** the kinetic model documented by the state diagram (Fig. 2c), its analytic solution (Eq. 5), and parameters (Supplementary Tables 1 and 2);
- **ii.** the crystal structural models of the three conformational states of RCK (PDB 1LNQ and 2FY8);
- **iii.** the state-specific orientations of helix αB that directly link the corresponding states in the structural and kinetic models.

A spatiotemporal model for the whole MthK channel

We previously predicted the Ca^{2+}-dependent p_o of the MthK channel from an energetic model, in which the regulatory module operates primarily in configuration *a* under low Ca^{2+} conditions and configuration *b* under high Ca^{2+} conditions[5] (Supplementary Fig. 1). In both configurations, all RCK domain in the open species adopt S_2. However, in configuration *a*, the eight RCK domains can independently adopt any of the three conformations, yielding more than six thousand closed species (without considering Ca^{2+}). A channel would thus spend the vast majority of time transitioning among closed species and rarely reach the open species. In contrast, in configuration *b*, each RCK can adopt only S_1 or S_3 in the closed state, yielding merely a few hundred closed species; a channel should thus spend much less time in the closed state than it would in configuration *a*.

Raising the Ca^{2+} concentration would both reduce the lifetime of S_1 or S_3 and promote configuration *b*, therefore dramatically shortening the lifetime of the channel's closed state, in agreement with previous electrophysiological studies[8, 9]. The lifetime of the channel's open state in the absence of Ca^{2+} is comparable to that of S_2 observed in the isolated regulatory module ($_{ch}\tau_o$ = 252±46 ms[9] versus $_a\tau_2$ = 241+12.7/-12.2 ms; Supplementary Table 3), whereas in near saturating Ca^{2+} conditions, it is comparable to the predicted lifetime for Ca^{2+}-bound S_2 in configuration *b* ($^{Ca}_{ch}\tau_o$ = 2030±332 ms[9] vs. $^{Ca}_{b}\tau_o$ = 2513+381/-775 ms; Supplementary Table 3; Supplementary Note 5). If these lifetimes of S_2 numerically reflect those of the channel's open state, then raising the Ca^{2+} concentration should modestly lengthen the open channel's lifetime, also in agreement with previous electrophysiological studies[8, 9].

In the framework of the energetic model and on the basis of RCK's kinetics, we derived the following two equations (Supplementary Note 6) to describe the Ca^{2+}-dependent lifetimes of the closed and open channel (τ_c and τ_o), which are quantitatively checked below against those previously observed (Fig. 5a):

$$ {}^{obs}\tau_c = \frac{\left(K+1+\left({}^{Ca}K+1\right)\frac{\left[Ca^{2+}\right]^{n_1}}{K_{D2}}\right)^m+\left(\frac{\left[Ca^{2+}\right]^{n_2}}{K_{Dn2}}\right)^m\left(K^m+{}^{ca}K^m\left(\frac{\left[Ca^{2+}\right]^{n_1}}{K_{D2}}\right)^m\right)}{\left((K+1)_ak_o+\left({}^{ca}K+1\right){}^{Ca}_ak_o\frac{\left[Ca^{2+}\right]^{n_1}}{K_{D2}}\right)\left(1+\frac{\left[Ca^{2+}\right]^{n_1}}{K_{D2}}\right)^{m-1}+\left(\frac{\left[Ca^{2+}\right]^{n_2}}{K_{Dn2}}\right)^m\left(K^m{}_bk_o+{}^{ca}K^m{}^{Ca}_bk_o\left(\frac{\left[Ca^{2+}\right]^{n_1}}{K_{D2}}\right)^m\right)}{}_gK \quad (8) $$

$$ {}^{obs}\tau_o = \frac{\left(1+\frac{\left[Ca^{2+}\right]^{n_1}}{K_{D2}}\right)^m+\left(\frac{\left[Ca^{2+}\right]^{n_2}}{K_{Dn2}}\right)^m\left(1+\left(\frac{\left[Ca^{2+}\right]^{n_1}}{K_{D2}}\right)^m\right)}{\left(k_2+{}^{Ca}k_2\frac{\left[Ca^{2+}\right]^{n_1}}{K_{D2}}\right)\left(1+\frac{\left[Ca^{2+}\right]^{n_1}}{K_{D2}}\right)^{m-1}+\left(\left[Ca^{2+}\right]^{n_2}\right)^m\left({}_bk_2+{}^{Ca}_bk_2\left(\frac{\left[Ca^{2+}\right]^{n_1}}{K_{D2}}\right)^m\right)} \quad (9) $$

where:

$$ K=\frac{[S_1]+[S_3]}{[S_2]} \text{ and } {}^{ca}K=\frac{\left[S_1\cdot Ca^{2+}\right]+\left[S_3\cdot Ca^{2+}_{n_1}\right]}{\left[S_2\cdot Ca^{2+}_{n_1}\right]} \quad (10) $$

and m is the number of RCK domains; ${}_gK$ is the apparent equilibrium constant of the channel gate[5], ${}_ak_o$ or ${}^{Ca}_ak_o$ is the reciprocal of the mean duration between the beginning of an S_2 event and the beginning of the next S_2 event, with or without Ca^{2+} bound (Supplementary Note 6, Eq. 47); ${}_bk_o$ or ${}^{Ca}_bk_o$ is the reciprocal of the mean duration between the end of an S_2 event to the beginning of the next S_2 event, with or without Ca^{2+} bound (Supplementary Note 6, underneath Eq. 48); and the values of n_1 and n_2 specify the number

of Ca^{2+} bound at distinct sites, among which the site denoted by n_1 may not necessarily be physically the same in configurations *a* and *b*[5].

The above expressions for ${}^{obs}\tau_c$ and ${}^{obs}\tau_o$ (Eqs. 8 and 9) lead to the equation that describes the dependence of the channel's p_o on the Ca^{2+} concentration (Eq. 15 in reference[5]). The curves calculated using these equations predict the experimentally observed relation between ${}^{obs}\tau_o$, ${}^{obs}\tau_c$ (Fig. 5a) or p_o (Fig. 5b) and the Ca^{2+} concentration within experimental errors[9]. Furthermore, we fitted Eq. 15 in reference[5], and rearranged versions of Eqs. 8 and 9 (Eqs. 56 and 57 in Supplementary Note 6) to the respective data sets. The fitted values, tabulated in Supplementary Table 4, were comparable to those used in above calculations (Supplementary Tables 1–3), such that the fitted curves, if plotted, would be visually indistinguishable from the corresponding calculated curves.

We now have the essential information to assemble an integrated model for the whole channel, defined by:

- **i.** the kinetic model documented by the state diagram (Supplementary Fig. 1), its analytic solutions (Eqs. 8 and 9), and parameters (Supplementary Tables 1–3);
- **ii.** the structural models documented by PDB 1K4C, 2FY8, and 3RBZ. Given that the model here requires at least two Ca^{2+}-binding sites per RCK, we used the PDB 3RBZ, in which Ca^{2+} ions bind each RCK domain in the open-state structure of the MthK channel at three sites[13]. A closed-state structure of the MthK pore is not yet available, and we thus used the closed-state structure of the pore domain from a different K^+ channel[14] (KcsA, PDB 1K4C) as a surrogate.
- **iii.** the state-specific orientations of helix αB that directly link the corresponding states of RCK in the structural and kinetic models.

We performed simulations to obtain the temporal templates for the integrated channel model, which would in turn further validate our kinetic model. For each condition, the overall simulation consisted of eight concurrent simulations for RCK domains and another one for the gate (Fig. 5c,d). For simplicity, the kinetics of the gate itself was assumed to follow the kinetics of the regulatory module during the transition between open and closed states. As an example, we show a 10-s segment in a 30 min simulation for the channel in 1 mM Ca^{2+} (observed EC_{50} = 0.97 mM)[5, 9], using the fitted values tabulated in Supplementary Tables 1–3 (Fig. 5d). The RCK domain's conformational states S_1, S_2 and S_3 are coded in different shades of yellow, blue and orange, respectively. An increase in the number of Ca^{2+} bound is indicated by a change of the color shade from a darker to a lighter one. Such an increase in the number of bound Ca^{2+} ions is coupled with a switch of the regulatory module from configuration *a* to *b* (depicted as a shift from the bottom half to the top, separated by a dashed line). The residence of the channel gate in open (dark blue) or closed (light blue) states is shown in the bottom panel.

As defined by the model, the open state occurs when all RCK domains adopt S_2. Also, as expected for a condition near EC_{50}, the gate was open about half of the time. We calculated open and closed times, as well as open probabilities, from the simulated time courses of the gate's conformational changes and compared them, point-by-point, with the previous

electrophysiology data[9]. The calculated values (open squares) matched those experimentally observed (closed circles) within experimental errors (Fig 5a, b). Thus, as demonstrated both analytically and numerically, we have developed a model that satisfactorily accounts for the kinetics of the MthK channel.

We generated movies of a full channel molecule in a Ca^{2+} concentration near its EC_{50}, featured in two views, along with the simulated time courses of individual RCKs and the channel gate (Supplementary Video 3); 16 consecutive frames from a short segment of the video are shown in Fig. 5e. The different behaviors of the molecule in three Ca^{2+} concentrations are compared in Supplementary Videos 4. These movies allow the visualization of the integrated mechanistic model of the channel that quantitatively account for the channel's spatiotemporal characteristics at the resolution and accuracy levels of the underlying studies.

Discussion

We have resolved the events of a single RCK domain transitioning among three conformational states, by monitoring state-specific spatial orientations of an α-helix attached with a fluorophore[4, 5]. We then used the time course of the orientation changes as a temporal template to link the three structure states and create a movie to exhibit a single RCK domain (Supplementary Video 1; Fig 1e).

Next, from the state connectivity and lifetimes of individual conformational events of RCK, we determined twelve rate constants of conformational transitions, along with three K_D values of Ca^{2+} binding (constrained with equilibrium analysis). These fifteen constants fully establish a six-state model that is minimally required to quantitatively account for RCK's multi-state kinetic behaviors. Furthermore, in the framework of an energetic model of the MthK channel[5], we deduced, from the kinetic characteristics of RCK, a model that quantitatively predicts the channel's kinetics within experimental errors. This predictability serves as a validation of not only this model but also our experimental approach. Despite working with the isolated regulatory module, introducing cysteine mutations, attaching the fluorophore, and anchoring the protein to a surface, the information necessary for deducing the kinetics of the whole channel was meaningfully preserved.

Finally, on the basis of state-specific spatial characteristics, we linked the present kinetic model and the available structural models together, to create an integrated spatiotemporal model of a whole channel. Thus, a combination of the present method and existing structural techniques, which are based on the efforts of numerous scientists, has now created an effective integrative version of dynamic structural biology, which should be applicable to studying a wide range of proteins.

Methods

Protein sample preparation and data collection

As described in reference[4], a recombinant protein of the MthK channel's regulatory module, which contained a N-terminal recognition sequence for biotin ligase, a C-terminal His-tag

with a preceding specific-protease-cutting sequence, and the double E146C and L153C mutation in helix αB, was produced using the bacterial BL-21 expression system. The protein was labeled with bifunctional rhodamine (Bis-((N-Iodoacetyl)-Piperazinyl)-Sulfonerhodamine; Invitrogen B10621) via the two mutant cysteine residues and attached to a coverslip conjugated with streptavidin (Arrayit) via biotinylated N-termini. Polarized emissions from individual bi-functional rhodamine labels, excited in the evanescent field created at the surface of the sample coverslip by circularly polarized laser beam (532 nm), were collected via a fluorescence microscope with four polarization emission channels onto an electron-multiplying charge-coupled device camera, while the sample protein was immersed in a solution containing 200 mM KCl, Ca^{2+} of various concentrations, and 10 mM HEPES titrated to pH 8.0, where 1 mM EGTA was used as a buffer in the nominal Ca^{2+}-free and low (0.1 mM) Ca^{2+} solutions.

Data collection and analysis

Also as described in reference[4], each intensity of the four emission components collected from a given fluorophore was a direct summation of individual pixels. I_{tot}, θ, φ, and Ω were calculated using Eqs. 62, 63, 61, and 70 in the Supplementary Note 3 and 6 in the above reference, respectively. Conformational transitions and states were identified in two separate steps. A *changepoint* algorithm was applied to the intensity traces to detect the transitions between conformational events, whereas a *k*-means-cluster-based algorithm was applied to identify the conformational states of individual events based on both θ and φ.

Data Availability

Data and materials described here will be made available upon reasonable request.

Supplementary Material

Refer to Web version on PubMed Central for supplementary material.

Acknowledgments

We thank Y. Zhou for technical support; Y. Jiang and R. MacKinnon for providing the cDNA of MthK; V. Pau and B. Rothberg for sharing their published data for comparison; and P. De Weer, T. Hoshi, and B. Salzberg for critiques of our manuscript at different stages of its development. This study was supported by the grant GM055560 from the National Institute of General Medical Sciences of the National Institutes of Health to Z. L.

Reference List

1. Coontz R, Fahrenkamp-Uppenbrink J, Lavine M, & Vinson V Going from strength to strength. Science 343, 1091 (2014). [PubMed: 24604190]
2. Murata K & Wolf M Cryo-electron miscroscopy for strcutural analysis of dynamic biological macromolecules. Biochim. Biophys Acta - General Subject 1862, 324–334 (2018).
3. Stryer L Fluorescence energy transfer as a spectroscopic ruler. Annual Review of Biochemistry 47, 819–846 (1978).
4. Lewis JH & Lu Z Resolving angstrom-scale protein-conformational changes by analyzing fluorescence anisotropy. Nat. Struct. Mol. Biol 26,802–807 (2019). [PubMed: 31488909]
5. Lewis JH & Lu Z Energetics of angstrom-scale conformational changes in an RCK domain of the MthK K^+ channel. Nat. Struct. Mol. Biol 26,808–815 (2019). [PubMed: 31488910]

6. Jiang Y et al. Crystal structure and mechanism of a calcium-gated potassium channel. Nature 417, 515–522 (2002). [PubMed: 12037559]
7. Ye S, Li Y, Chen L, & Jiang Y Crystal structures of a ligand-free MthK gating ring: insights into the ligand gating mechanism of K^+ channels. Cell 126, 1161–1173 (2006). [PubMed: 16990139]
8. Zadek B & Nimigean CM Calcium-dependent gating of MthK, a prokaryotic potassium channel. J. Gen. Physiol 127, 673–685 (2006). [PubMed: 16735753]
9. Pau VP, Barca-Heidemann K, & Rothberg BS Allosteric mechanism of Ca^{2+} activation and H^+-inhibited gating of the MthK K^+ channel. J. Gen. Physiol 135, 509–526 (2010). [PubMed: 20421375]
10. Sakmann B & Neher E Single-Channel Recording (Plenum Press,1995).
11. Miller C Ion channel reconstitution (Plenum, New York, 1986).
12. Lewis JH, Jamiolkoski RM, Woody E, Ostap EM, & Goldman YE Deconvolution of camera instrument response functions. Biophys J. 112, 1214–1220 (2017). [PubMed: 28355548]
13. Pau VP et al. Structure and function of multiple Ca^{2+}-binding sites in a K^+ channel regulator of K^+ conductance (RCK) domain. Proc. Natl. Acad. Sci. U. S. A 108, 17684–17689 (2011). [PubMed: 21997217]
14. Zhou Y, Morais-Cabral JH, Kaufman A, & MacKinnon R Chemistry of ion coordination and hydration revealed by a K^+ channel-Fab complex at 2.0 A resolution. Nature 414, 43–48 (2001). [PubMed: 11689936]

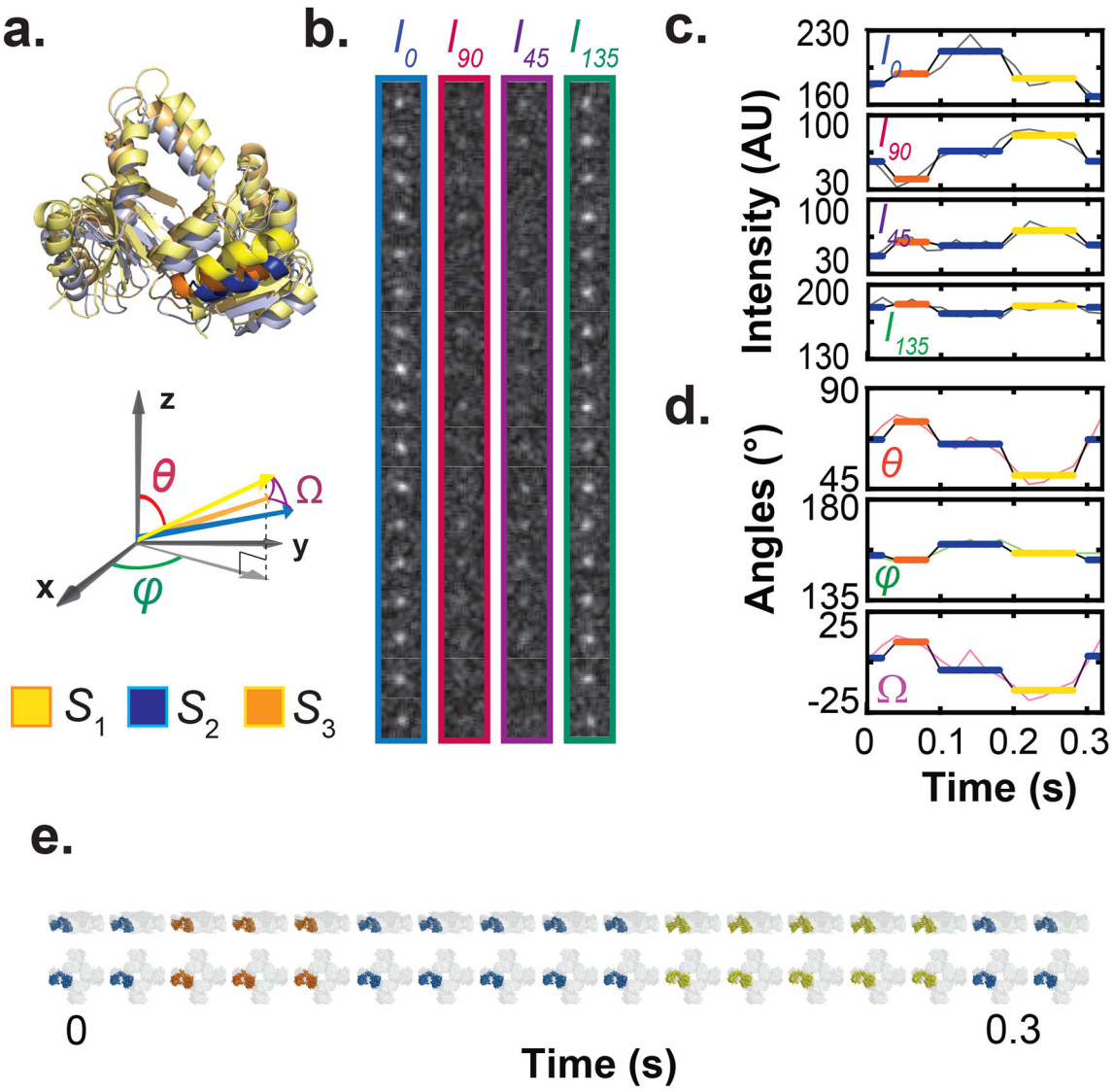

Figure 1.

Structures of RCK, polarized-fluorescence intensities, dipole orientations of a fluorophore, and movie frames for the tracked RCK. **a**. Three RCK conformations are aligned and the α-helix under examination is color-coded as indicated below; the color scheme for S1, S2 and S3 states is used throughout. The reference coordinates are shown below the structures. **b**. Consecutive 17 frames of four intensity components (I_0, I_{45}, I_{90} and I_{135}) recorded from a fluorophore attached to a single RCK domain at a constant interval of 20 ms per frame during a selected 0.3-sec segment of a ~4-sec recording. **c**. Intensity values were integrated from the 17 images shown in **b** and plotted against time. **d**. Values of θ and φ calculated from the four intensity traces (**c**) and values of Ω calculated relative to S_2. In panels **c** and **d**, transition points of the colored traces superimposed on the records were determined by a c*hangepoint* analysis, and the constant values between transition points are arithmetic means of the observed data. **e**. Consecutive frames of Supplementary Video 1 of RCK conformational changes where the three conformations tracked RCK is represented by the

corresponding electron density maps (PDB 1LNQ and 2FY8)[6, 7], in accordance with the temporal information of the *Ω* trace (**d**). The tracked RCK is presented against a contour of the regulatory module in a side view of the regulatory module (top) or in a view along its central axis (bottom).

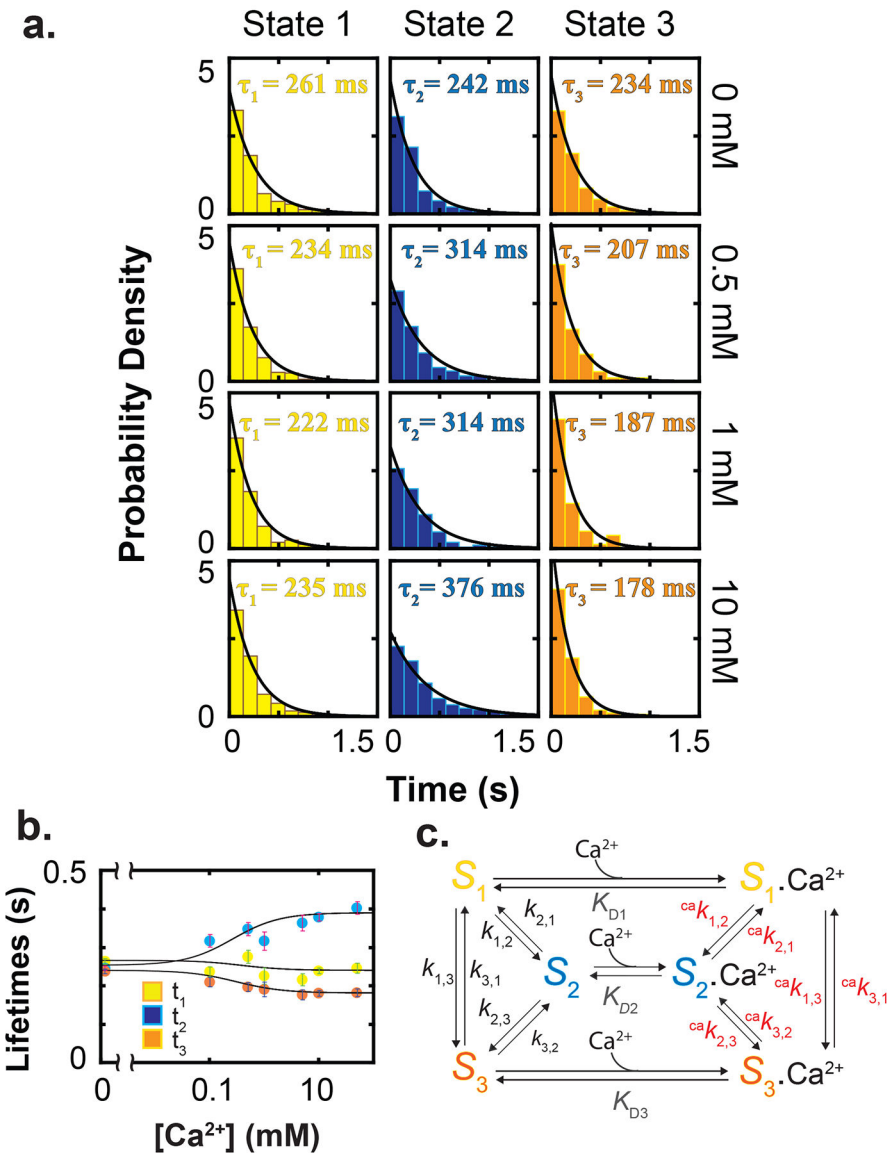

Figure 2.

Observed dwell-time distributions and lifetimes of RCK conformations, and a kinetic model of RCK. **a**. Dwell time distributions of the three conformational states, obtained in the presence of four indicated Ca^{2+} concentrations. The curves superimposed on the data were calculated from lifetimes using a single exponential function as described in the text. **b**. Lifetimes (mean ± s.e.m, 20 – 1003 events per distribution) of individual states in the presence of various Ca^{2+} concentrations, calculated from the observed dwell times. The curves superimposed on the data correspond to Eq. 17 (Supplementary Note 3). **c**. State diagram of a kinetic model of RCK, based on an energetic study[5], where K_{Di} and rate constants of individual state transitions are denoted.

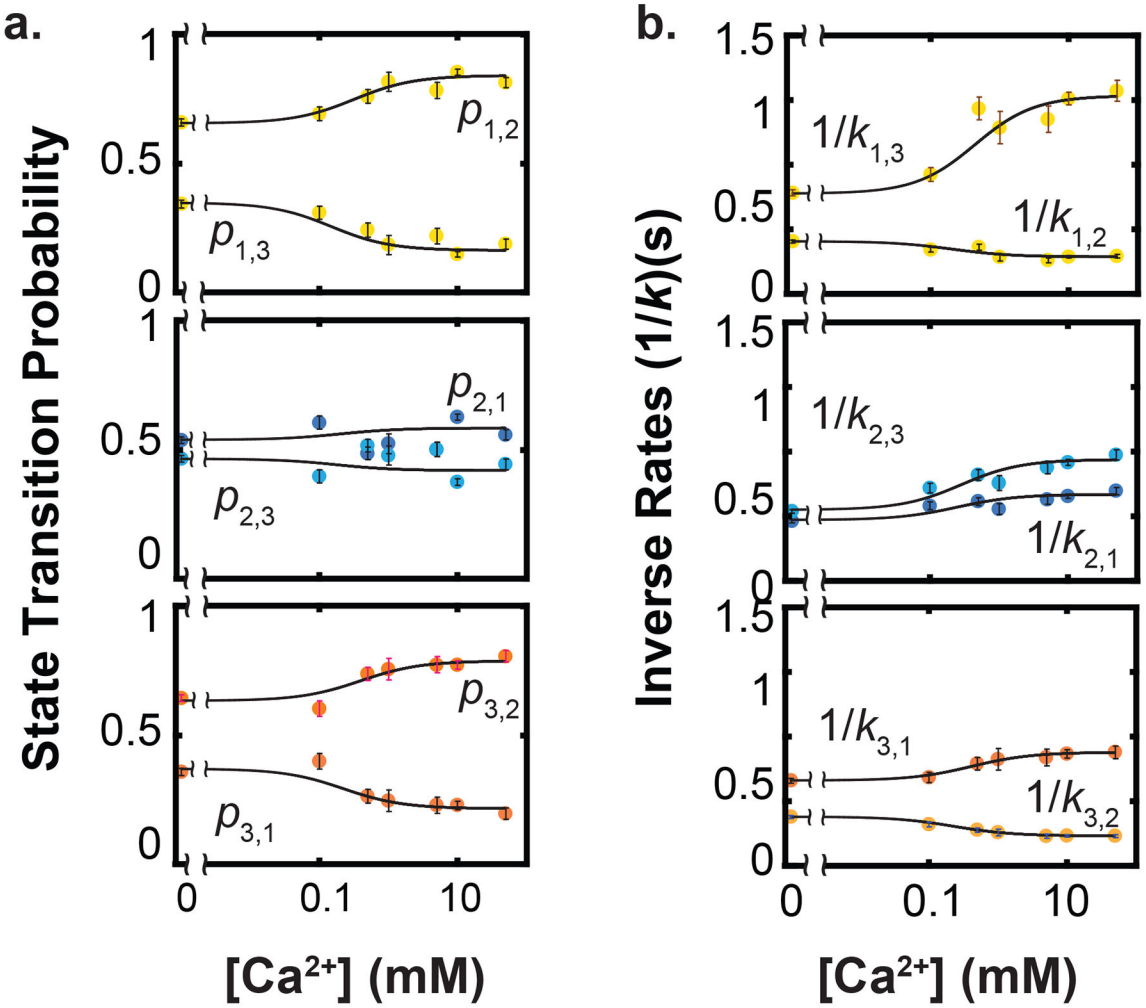

Figure 3.

Probabilities and rate constants of state-to-state transitions. **a**, **b**. The probabilities and rate constants (mean ± s.e.m, 20 – 1003 events per distribution) over a range of Ca^{2+} concentrations, calculated using Eqs. 3 and 4. The curves superimposed on the data correspond to a global fit of an equation in the form of Eq. 17 (Supplementary Note 3) with the rate constants being replaced by the probabilities of state-to-state transitions (**a**) and Eq. 5 (**b**); the fitted values are presented in Supplementary Tables 1 and 2.

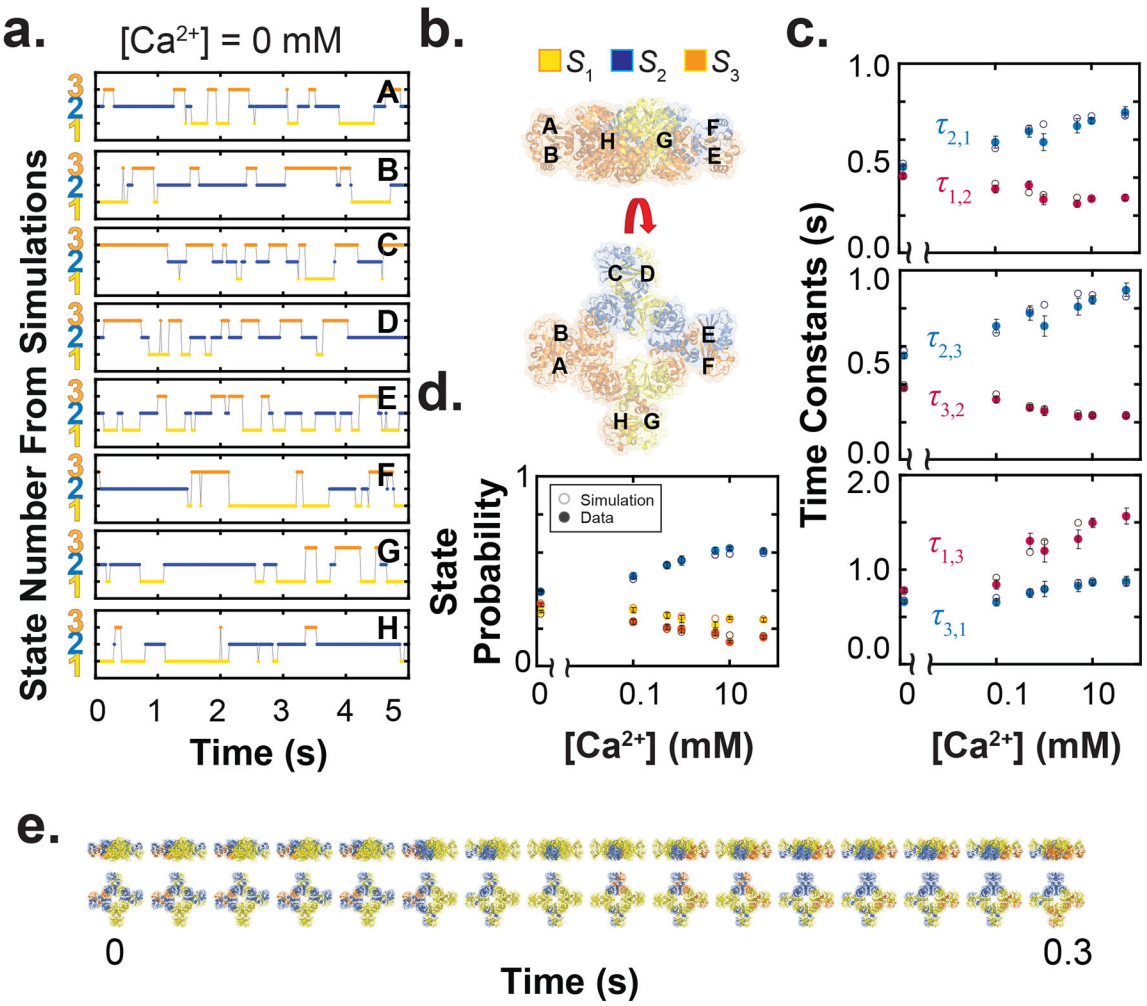

Figure 4.

Simulated kinetics and movie frames for individual RCKs in the isolated regulatory module. **a**, **b**, Concurrent simulations of state transition kinetics of eight independent RCKs for a Ca^{2+}-free condition (**a**, A-H) as assigned in the structure model (**b**), created according to the three conformations documented in PDB 1LNQ and 2FY8 and shown in a side view (upper) and a view along its central axis (lower); individual states are color coded as indicated. **c**, **d**. Time constants for individual state-to-state transitions and the probabilities of RCK's three conformational states calculated from simulated data (open symbols), compared to experimentally observed data points (closed symbols; mean ± s.e.m, 20 – 1003 events per distribution). **e**. Consecutive frames of a movie segment of the regulatory module in the two views (Supplementary Video 2), generated as described in the text.

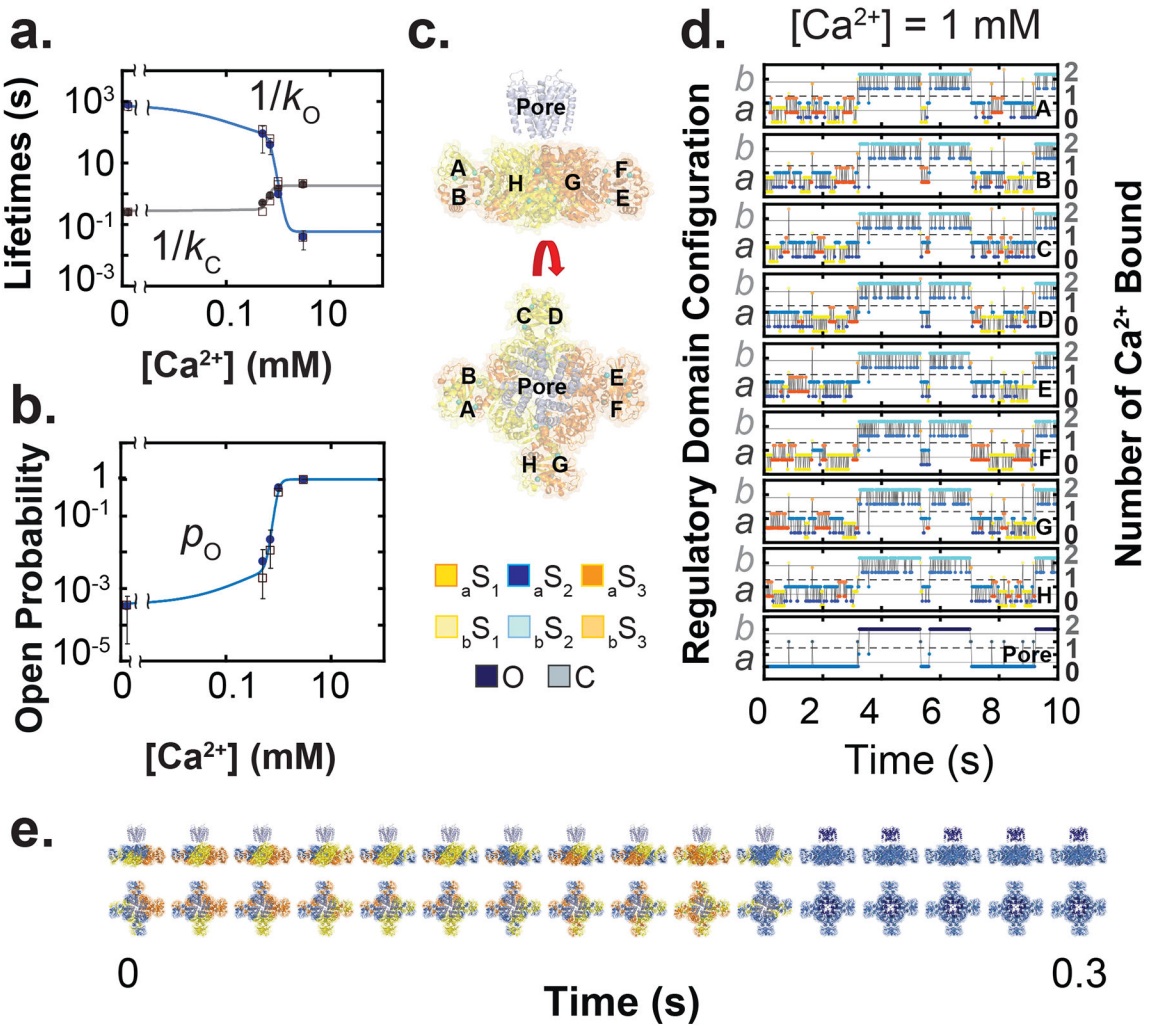

Figure 5.

Comparison of the kinetic model with the observed data, simulated kinetics and movie frames for a whole channel. **a,b**. The open and closed lifetimes (**a**), as well as open probabilities (**b**), of the channel, calculated from simulated points (open symbols), are compared to previous experimentally observed data points[9] (mean ± s.e.m; closed symbols). The observed lifetimes τ_o and τ_c are so-called Ca^{2+}-dependent 'burst' and 'gap' times. The curves in **a** or **b** were calculated with Eqs. 8 and 9 or Eq. 15 in reference[5], respectively (see Supplementary Tables 1–3 for parameter values). $_gK$ was set to value of 1.7, and n_2 to 1 (reference[5]); all parameters obtained from RCK were taken from Supplementary Tables 1–3. **c**. A crystal structure model is shown in a side view (upper) and a view along its central axis (lower), created as described in Fig. 4; the color-coding for RCK states is shown below. **d**. Concurrent simulations of state kinetics for eight RCK domains (A-H as assigned in **c**), where S_1, S_2 and S_3 are color coded in shades of yellow, blue and orange, respectively; the shade changes from a darker to a lighter one when the number of Ca^{2+} bound increases, as indicated on the right *y*-axis. Configuration *a* or *b*, indicated on left y-axis, occupies the lower or upper half of each panel, separated by a dashed line. The residence of the gate in open (dark blue) and closed (light blue) states is shown in the bottom panel. **e**. Consecutive

frames of a movie segment of a whole channel model in the two views (supplementary movie 3) generated as described in the text.